THE JOURNAL OF PHYSICAL CHEMISTRY B

ARTICLE

pubs.acs.org/JPCB

Driving Force for Hydrophobic Interaction at Different Length Scales

Ronen Zangi*

Department of Organic Chemistry I, University of the Basque Country UPV/EHU, Avenida de Tolosa 72, 20018, San Sebastian, Spain, and IKERBASQUE, Basque Foundation for Science, 48011, Bilbao, Spain

Supporting Information

ABSTRACT: We study by molecular dynamics simulations the driving force for the hydrophobic interaction between graphene sheets of different sizes down to the atomic scale. Similar to the prediction by Lum, Chandler, and Weeks for hard-sphere solvation [*J. Phys. Chem. B* **1999**, *103*, 4570−4577], we find the driving force to be length-scale dependent, despite the fact that our model systems do not exhibit dewetting. For small hydrophobic solutes, the association is purely entropic, while enthalpy favors dissociation. The latter is demonstrated to arise from the enhancement of hydrogen bonding between the water molecules around small hydrophobes. On the other hand, the attraction between large graphene sheets is dominated by enthalpy which mainly originates from direct solute−solute interactions. The crossover length is found to be inside the range of 0.3−1.5 nm^2 of the surface area of the hydrophobe that is eliminated in the association process. In the large-scale regime, different thermodynamic properties are scalable with this change of surface area. In particular, upon dimerization, a total and a water-induced stabilization of approximately 65 and 12 kJ/mol/nm^2 are obtained, respectively, and on average around one hydrogen bond is gained per 1 nm^2 of graphene sheet association. Furthermore, the potential of mean force between the sheets is also scalable except for interplate distances smaller than 0.64 nm which corresponds to the region around the barrier for removing the last layer of water. It turns out that, as the surface area increases, the relative height of the barrier for association decreases and the range of attraction increases. It is also shown that, around small hydrophobic solutes, the lifetime of the hydrogen bonds is longer than in the bulk, while around large hydrophobes it is the same. Nevertheless, the rearrangement of the hydrogen-bond network for both length-scale regimes is slower than in bulk water.

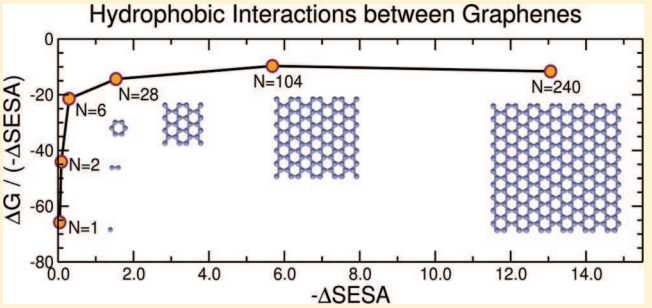

I. INTRODUCTION

Hydrophobic interactions, or the attractive forces between nonpolar groups in water, play an important role in many phenomena in nature, for example, in micelles and cell membrane formation, acceptor−ligand binding, and stability of protein structures.[1] Nevertheless, for a long time the notion of hydrophobicity has been elusive. This was mainly due to the realization that the forces acting between hydrophobes are, in part, not direct forces between particles, but are rather induced by the surrounding aqueous medium. Water is famous for its extensive network of hydrogen bonds. These hydrogen bonds are much stronger than other intermolecular interactions, rendering water an associative liquid. Consequently, one would think that the attractive force between two nonpolar solutes in water originates from the inability of water molecules next to the solute to form as many hydrogen bonds as it can in bulk water.[2] However, measurements of the thermodynamics of solvation demonstrated that the forces between nonpolar organic compounds in water are induced by entropy,[3] and on the contrary, the change in enthalpy upon solvation of many small nonpolar solutes is negative.[4] This entropy-induced hydrophobicity is in line with the observation that the strength of the hydrophobic interaction increases with temperature.

These developments were taken further by Frank and Evans[5] who proposed that water molecules around hydrophobic solutes arrange themselves in a quasi-crystalline structure, referred to as an "iceberg", in which there is less randomness. For many years, the idea of an iceberg surrounding apolar solutes has been fueling debates in the literature. In fact, as expressed by Blokzijl and Engberts,[4] the entire idea that the hydrophobic interactions are entropy driven "gave chemists a genuine feeling of discomfort". In 1973, Stillinger[6] proposed that water molecules around small hydrophobes can maintain their hydrogen bond network while around large hydrophobes they cannot, paving the road for introducing enthalpy as a second driving force for hydrophobic interactions. Lum, Chandler, and Weeks (LCW) quantified this idea through their theory of hydrophobic solvation.[7] They predicted that the crossover between small and large regime occurs on nanometer length scale. This crossover length is about the range of interactions between water molecules in the bulk. Subsequent computer simulations reported that the excess Gibbs (free) energy of solvation of small hard-sphere solutes (i.e., formation of cavities) in water scales

Received: September 21, 2010
Revised: January 20, 2011
Published: February 18, 2011

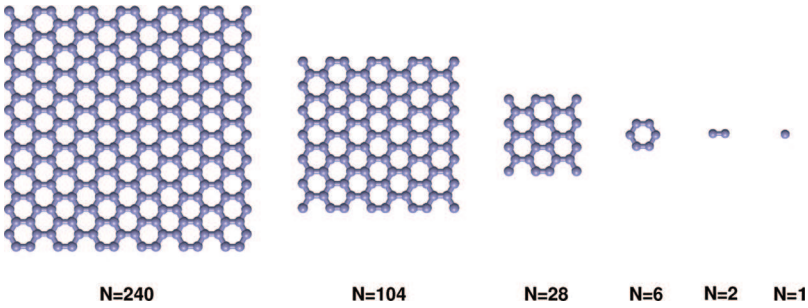

Figure 1. Models for hydrophobes of different sizes, and consequently different number of constituting atomic particles, N, prepared by rectangular cuts of a graphene sheet. See Table 1 for the rectangular dimensions of the $N \geq 28$ plates.

approximately with the solute's volume, whereas the excess Gibbs energy of large solutes scale with solute's surface area.[8,9] These results were also reproduced using scaled particle theory,[10] and in addition, it was argued that this crossover length also exists in other liquids.

Water exhibits many anomalous properties, in which many, if not all, can be attributed to the extent of its hydrogen bonding. The hydrophobic effect is of no exception; that means it can be attributed to the interruption of the hydrogen bond network by the hydrophobic solute. In the small-scale regime the hydrogen bonds are not lost but it cost entropy for water to maintain them. In the large-scale regime, the water hydrogen bond network cannot persist anymore and enthalpy is brought into play. What is the origin of the entropy loss of water next to small hydrophobes? Certainly the term "iceberg" should not be understood as if ice layers are surrounding the hydrophobes. Even the formation of a rigid clathrate-like structure is controversial.[11−13] Other arguments state that the possible configurations of hydrogen bonding between water molecules next to small hydrophobes are restricted.[14,15] Although this is reasonable, it has not been demonstrated yet. It is also intriguing to know whether the same physical picture for the reduced entropy is applicable next to large hydrophobes.

In this paper, we study the behavior of the hydrophobic interaction between graphene sheets of varying sizes. As was found for the solvation of hard-sphere solutes,[7−9] we observe the mechanism for association to be length-scale dependent. The crossover length is found to be in the range of 0.3−1.5 nm^2 of the surface area of the hydrophobe that is eliminated in the process. The attractive force between small hydrophobes is induced purely by entropy. In fact, the enthalpic part of the Gibbs energy opposes association. This is because the number of hydrogen bonds between water molecules surrounding small hydrophobes is larger than in bulk water. On the other hand, for large sheets the association is driven by both enthalpy and entropy with relative contributions of 7 and 3, respectively, to the change in the Gibbs energy. In this large-scale regime, the Gibbs energy of association, as well as other thermodynamic properties, scale as the change in the surface area of the hydrophobe exposed to the solvent. The difference between small- and large-scale association is the inability of the water molecules to maintain their hydrogen bond network next to large surface, and indeed, we find that on average one hydrogen bond is broken around 1 nm^2 of hydrophobic surface. The potential of mean force between large graphene sheets is also scalable, except for interplate distances smaller than 0.64 nm, which corresponds to the barrier of removing the last water layer. For larger sheets, a relatively lower barrier height for association and larger range of attraction are observed. We further show that the dynamics of the hydrogen bonds around small solutes is different from that around large solutes. Hydrogen bonds around small hydrophobes live longer than in the bulk, explaining the larger number of hydrogen bonds found around these solutes. The rearrangement of hydrogen bonds is also retarded in this case. On the other hand, around large hydrophobes, the hydrogen bond lifetime is similar to that in the bulk; however, the dynamics of rearranging the network is slower.

II. METHODS

We study the driving force for the hydrophobic interaction between two identical nonpolar hydrophobes of varying sizes. The four largest hydrophobes (see Figure 1) are represented by a graphene sheet that was prepared by cutting a rectangle from a monolayer of hexagonal graphite structure with bond length of 0.142 nm. The smallest (described by a single atom, $N = 1$) and the second smallest ($N = 2$) hydrophobes cannot be considered as sheets of graphene; however, all the parameters taken (the LJ values and the bond length) are the same as those used to describe the graphene sheets. This was done in order to elucidate the driving force of the hydrophobic association down to the atomic scale, keeping the "chemical identity" of the constituting carbon unit the same. The carbon−water Lennard-Jones (LJ) parameters, $\sigma_{co} = 0.319$ nm and $\varepsilon_{co} = 0.392$ kJ/mol, were taken from parametrization of the contact angle of water on graphite.[16] These values were also used to extract the LJ parameters (using the geometric combination rule) between two graphene carbon atoms. During simulations, the positions of the hydrophobe atoms are held fixed, interactions between atoms on the same hydrophobe are excluded, and the orientation of the two planes of the sheets (or the two bond vectors for $N = 2$) is parallel and in-registry with respect to each other.

We used the molecular dynamics package GROMACS version 4.0.5[17] to perform all of the computer simulations with a time step of 0.002 ps. In all cases, we solvated the two hydrophobes in 1520 water molecules described by the TIP4P-Ew model.[18] Their bond distances and angle were constrained using the SETTLE algorithm.[19] The electrostatic forces were evaluated by the particle-mesh Ewald method (with real-space cutoff of 1.0 nm, grid spacing of 0.12 nm, and quadratic interpolation) and the LJ forces by a cutoff of 1.0 nm (with long-range dispersion corrections for the energy and pressure). The system was maintained at a constant temperature of 300 K by the velocity rescaling thermostat[20] and at a pressure of 1.0 bar by the Berendsen thermostat.[21]

The potential of mean force (PMF) between the two hydrophobes was computed from the mean force acting on each of the

hydrophobes.[22,23] Then the mean force acting between the hydrophobes along their axis of separation (the z-axis) was integrated as a function of the distance between the hydrophobes, d, to yield the Gibbs energy profile. As the PMF represents only relative values, it was shifted such that the Gibbs energy of the state at the largest separation (d = 1.86 nm) corresponds to zero. To obtain the PMF for each hydrophobe, we performed 70 simulations with different values of d, ranging from 0.26 to 1.86 nm. At each distance, the system was equilibrated for 6.0 ns and data collected for an additional 18.0 ns. The error in the quantities obtained from the simulations was estimated using the block averaging method.[24] The error in determining the change in Gibbs energy, ΔG, between the associated (d = 0.31 or 0.32 nm) and dissociated (d = 1.86 nm) states is obtained by integrating the mean forces plus/minus their errors.

In order to achieve accurate analyses of the system at the associated and dissociated states, we performed six additional simulations at each of these points for 42.0 ns (thus, a combined trajectory of 252.0 ns) for each N. This was necessary since the change in enthalpy, which is calculated from the change in the potential energy of the system, $\Delta H = \Delta U + p\Delta V$, is obtained by subtracting a large number from a similar large number. These six simulations were considered statistically independent and therefore, the error estimate in this case was determined by the standard error of the mean (obtained from the six simulations). Note that the magnitude of the error calculated for ΔU is at least 2 orders of magnitude larger than the term $p|\Delta V|$ and, therefore, the latter can be safely ignored. We also run at d = 0.60 nm and d = 0.70 nm 12 and 6, respectively, additional simulations of 42.0 ns each to obtain accurate density profiles of the oxygen atoms of the water molecules along the z-axis, the axis perpendicular to the plane of the graphene sheets.

We define the change in the solvent-excluded surface area, ΔSESA, for the association reaction as the surface area of the hydrophobe exposed to the solvent in its dimeric state minus the SESA of the two monomers. Since for dimerization, this yields negative values for ΔSESA, we plotted the different thermodynamic properties as a function of $-\Delta$SESA. The calculations of the SESA for the associated and dissociated states were performed using the MSMS program.[25] The effective diameter between the carbon atom and the probe solvent molecule were taken form the location of the first maximum (r = 0.328 nm) in the carbon(hydrophobe)−oxygen(water) radial distribution function (RDF).

Two water molecules were considered to be hydrogen bonded if the hydrogen−oxygen distance was smaller than 0.244 nm (the first minimum in the corresponding bulk RDF), and the donor−hydrogen−acceptor connectivity angle was larger than 150°. The dynamics of the hydrogen bond lifetime between water molecules around the hydrophobes was calculated by two different autocorrelation functions[26,27]

$$C_{HB}(t) = \frac{\langle h(0)h(t)\rangle}{\langle h\rangle} \quad (1)$$

$$S_{HB}(t) = \frac{\langle h(0)H(t)\rangle}{\langle h\rangle} \quad (2)$$

The average in eqs 1 and 2 includes all pairs of water molecules inside the first solvation shell of the hydrophobe. This was determined by a cutoff distance of 0.50 nm between the oxygen atom of water and the closest atom of the hydrophobe, a distance equal to the location of the first minimum in the corresponding RDF. The value of $h(t)$ equals 1 if a particular pair of water molecules is hydrogen bonded at time t, and otherwise 0. On the other hand, $H(t)$ equals to 1 only if a particular pair of water molecules is continuously hydrogen bonded from time 0 to t. Thus, the autocorrelation function $S_{HB}(t)$ does not consider reforming of bonds after they broke at intermediate times, while $C_{HB}(t)$ does.

Table 1. Solvent-Excluded Surface Area (in nm^2) of the Different Hydrophobe (Graphene Sheet) Systems, Calculated for the Monomeric and Dimeric States as Well as for the Change in the Association Process[a]

N (carbons)	$x \times y$	2 × SESA (monomer)	SESA (dimer)	$-\Delta$SESA
1		0.678	0.633	0.045
2		0.967	0.881	0.086
6		1.761	1.470	0.291
28	0.710 × 0.738	5.681	4.145	1.536
104	1.562 × 1.476	16.173	10.490	5.683
240	2.414 × 2.338	33.208	20.150	13.058

[a] For $N \geq 28$, the x and y dimensions of the rectangular plate (in nm), as measured by the center to center distance between two end atoms, are also given.

III. RESULTS AND DISCUSSION

The models of the different hydrophobes used in this study are plotted in Figure 1. In these models, the number of graphene carbon atoms, N, for each monomer range from 1 to 240. The process that we are considering is the association (dimerization) of two identical hydrophobes (H)

$$H + H \rightleftharpoons H_2 \quad (3)$$

It is likely that, for large N, the thermodynamic properties of the hydrophobic interactions will scale as a function of the size of the area (of the hydrophobes) exposed to the solvent that is buried in the association process. We computed the solvent-excluded surface area for both sides of eq 3 and the corresponding change, ΔSESA, for dimerization. For simplicity, we will use the value of $-\Delta$SESA as the scaling factor since it is positive for eq 3. The results are shown in Table 1. In this range of model hydrophobes, the change in the solvent-excluded surface area spans more than 2 orders of magnitude.

The potential of mean force (PMF) of bringing the two hydrophobes from far apart into contact is displayed in Figure 2. The upper and middle panels present, respectively, the total (direct + induced) and induced PMFs. Important values derived from these PMFs are given in Table 2. Specifically, the table indicate explicitly the direct solute−solute, and solvent-induced, contributions to the Gibbs energy of forming the contact and first solvent-separated states, as well as, of the barrier height between these two states relative to the first solvent-separated state (i.e., the barrier for removing the last water layer). The results shown in Table 2 indicate that the relative contribution of the solvent-induced interactions to the stability of the contact state is largest for N = 1 and gradually decreases with N. For example, it is 100% for N = 1 while only 19% for N = 240. In fact, for N > 28 the major

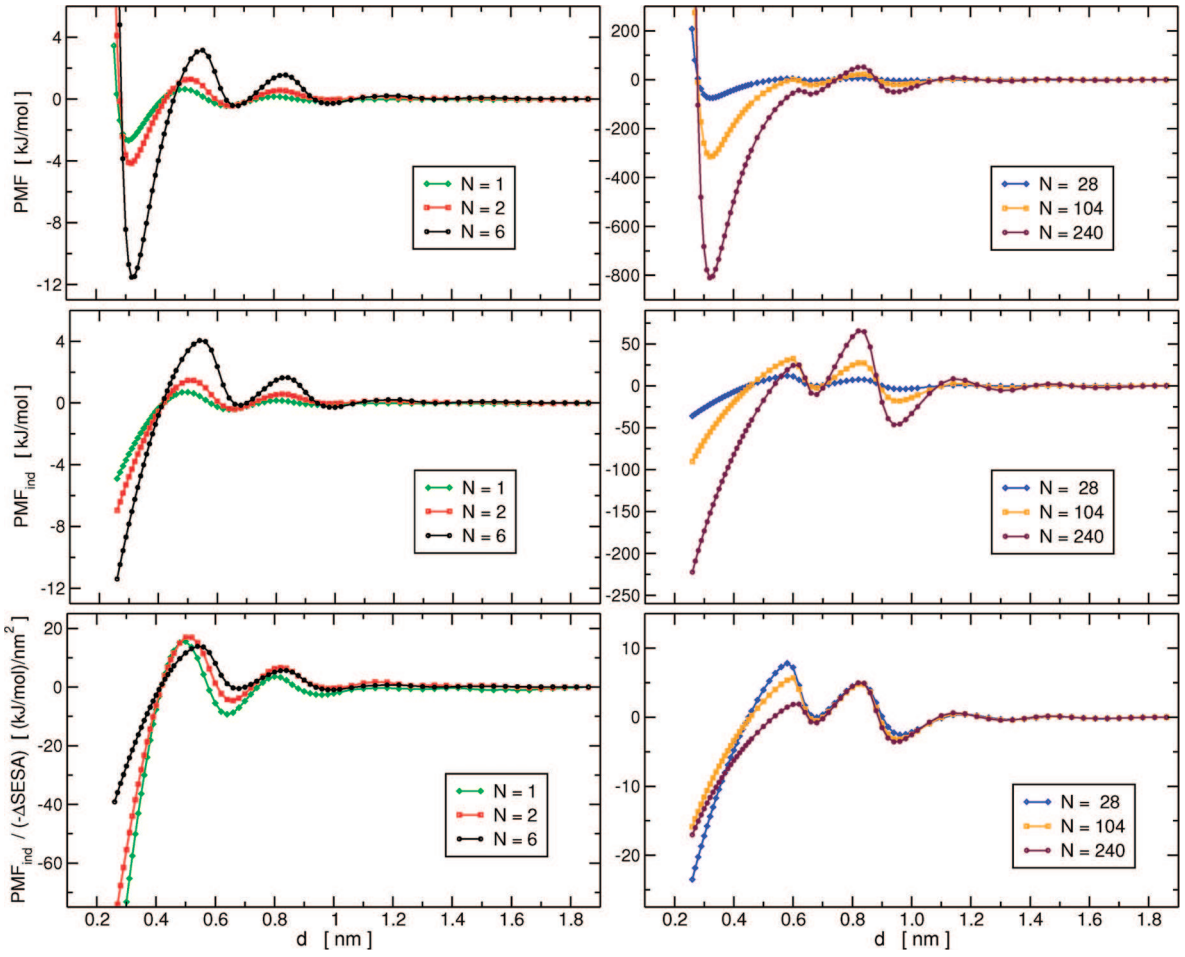

Figure 2. Upper and middle panels: The total and induced potential of mean force, respectively, between two identical hydrophobes as a function of the distance between their center of mass, d, for different model systems. The long axis of the hydrophobe (for $N = 2$), or the planes of the two graphene sheets (for $N > 2$), are parallel and in-registry with respect to each other. In all cases, the equilibrium distance for the contact state occurs at $d = 0.32$ nm, except for $N = 1$ where the minimum of the curve is at $d = 0.31$ nm. Lower panel: The induced PMFs scaled by the change in the surface area of the hydrophobes exposed to the solvent ($-\Delta$SESA).

Table 2. Summary of the Important Features of the PMFs Shown in Figure 2[a]

	contact state		FSS state		barrier height	
N (carbons)	direct	induced	direct	induced	direct	induced
1	0.3	−3.0	−0.01	−0.4	−0.05	1.1
2	−0.4	−3.8	−0.04	−0.4	−0.1	1.9
6	−5.3	−6.2	−0.3	−0.2	−0.7	4.2
28	−52.8	−22.1	−3.2	−0.02	−3.8	12.0
104	−259.5	−55.0	−16.6	−2.5	−14.2	34.9
240	−658.0	−151.8	−42.7	−10.4	−25.0	35.3

[a] Direct solute−solute, and solvent-induced, contributions to the Gibbs energy of forming the contact and first solvent-separated (FSS) states, as well as, of the barrier height between these two states relative to the FSS state are shown. All numbers are given in kJ/mol.

part of the stabilization of the contact pair is from direct solute−solute interactions. In all cases, except for $N = 1$, the minimum of the total PMF curve, which marks the equilibrium state for association, is at $d = 0.32$ nm, while for $N = 1$ it is at $d = 0.31$ nm. In earlier investigations, it has been observed that two hydrophobic surfaces that are brought into contact can display a drying transition (at gap separations that can hold at least two water layers) where the water confined between the two surfaces is unstable in its liquid state and evaporates.[28−32] However, for graphene sheets the hydrophobe−water interaction is too strong to support this transition,[33,34] and accordingly, drying was not observed in any of the cases studied. In the lower panel of Figure 2, the induced PMFs scaled by $-\Delta$SESA are shown. For the systems $N = 1$, 2, and 6 the PMFs are not scalable, but they are all characterized by a relatively large barrier for association. For $N = 28$, 104, and 240, the PMFs are scalable, except in the region $d < 0.64$ nm, where the curves with larger N have a relatively lower barrier for association and larger range of attraction (the latter property is actually true for all N). The significance of the scaled PMFs of the different model systems to produce a single curve is that a PMF of one system can be predicted from the PMF of another system. The results indicate that for the plates we study here with $N = 28$, 104, and 240 this can be done down to the interplate distance $d = 0.64$ nm, where smaller values correspond to the ejection of the last water layer. See below for an analysis on the origin of this phenomenon. Note that the $N = 6$ and $N = 28$ PMFs are not scalable (figure is not shown).

Table 3 presents the results of the thermodynamics of the association process. The Gibbs energy change, ΔG, is computed

Table 3. Thermodynamic Data for the Association Process of Two Identical Hydrophobes[a]

N (carbons)	ΔG	ΔH	$T\Delta S$	driving force for association
1	-2.7 ± 0.4	2.4 ± 0.8	5.1 ± 1.2	100% entropic
2	-4.2 ± 0.5	4.2 ± 0.9	8.4 ± 1.4	100% entropic
6	-11.5 ± 0.6	3.7 ± 1.1	15.2 ± 1.7	100% entropic
28	-74.9 ± 0.9	-23.1 ± 1.0	51.8 ± 1.9	31% enthalpic and 69% entropic
104	-314.5 ± 1.4	-200.8 ± 1.1	113.7 ± 2.5	64% enthalpic and 36% entropic
240	-809.7 ± 4.0	-563.2 ± 1.4	246.5 ± 5.4	70% enthalpic and 30% entropic

[a] All energy units are in kJ/mol.

by the difference of the value of the PMF in the dissociated state (d = 1.86 nm) from that in the associated state (d = 0.31 nm for N = 1, and d = 0.32 nm otherwise). In all cases, ΔG is negative which means the systems favor association. The change in enthalpy, ΔH, is calculated from the change in the potential energy (the magnitude of the volume change between the two states would make a negligible contribution to ΔH), and the change in entropy was calculated from $T\Delta S = \Delta H - \Delta G$. The results shown in Table 3 indicate that for N = 1, 2, and 6 the driving force for hydrophobic association is purely entropic. In fact, the change in enthalpy, as was found by experiments,[4] favors dissociation; however, it is overcome by the entropy change. On the other hand, for $N \geq 28$, both entropy and enthalpy contribute to the association of the hydrophobes. As the surface area of the hydrophobe increases (i.e., for larger N), the relative contribution of the enthalpy to drive the association increases, and for N = 240, 70% of the Gibbs energy for dimerization is enthalpic. We suspect that for larger N, not too far from N = 240, the relative contribution of enthalpy and entropy will remain constant. [This is because, once the fraction of the edge particles is negligible, the number of water molecules that are perturbed due to the graphene sheets will be proportional to the surface area of the hydrophobe exposed to the solvent, and all changes in thermodynamic properties will scale accordingly.] Note that the crossover in the driving force for hydrophobic interaction, from purely entropic at small length scale of the hydrophobes to being dominated by enthalpy for large hydrophobes, is in line with theoretical predictions.[6,7] Furthermore, the location of the crossover occurs for a value of $0.3 < -\Delta\text{SESA} < 1.5$ nm^2, which is on the same order as the crossover radius of 0.5−1 nm obtained from the LCW theory,[8,9] although this theory considered solvation of hard objects that at large scale exhibit a drying transition.

As mentioned above, for large N, the change in Gibbs energy for association is expected to scale as the surface area of the hydrophobe that is eliminated in the process. This is true as long as the thickness of the hydrophobe−water interface does not change with the size of the graphene sheets. The PMF and, consequently, the Gibbs energy change of the reaction can be decomposed into a direct and an induced part (see below). Figure 3a displays the curves of the total and induced changes in Gibbs energy as a function of $-\Delta$SESA. The scaling of $\Delta G_{\text{induced}}$ by $-\Delta$SESA yields a plateau for large N. The plateau region starts around N = 28, the size of hydrophobe which marks the onset of the large scale behavior detected in Table 3 based on the entry of the enthalpy as a driving force for association. However, $\Delta G_{\text{total}}/(-\Delta\text{SESA})$ does not (yet) display a plateau. The reason is that the size of plates we used in the simulations are too small for the direct part of the Gibbs energy change to scale as the surface area of the graphene sheets. The value of ΔG_{direct} equals the potential energy interaction between the sheets in the

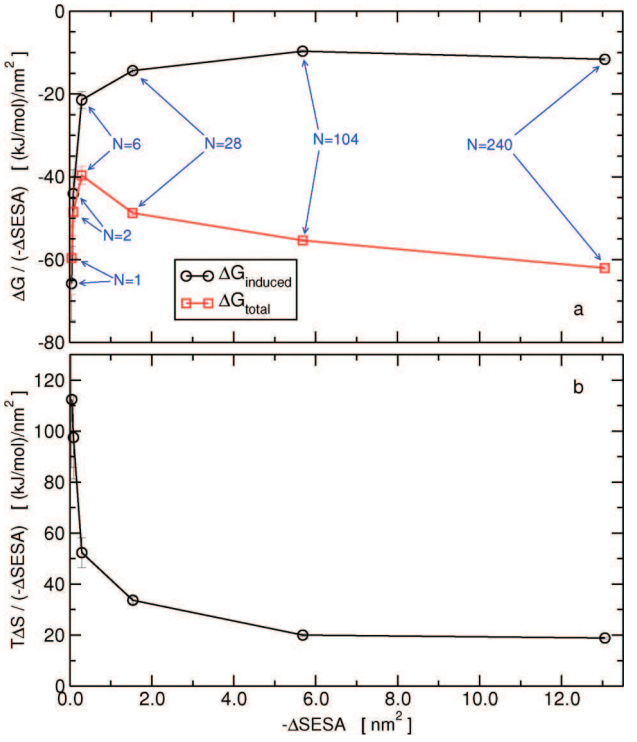

Figure 3. (a) Total and the induced Gibbs (free) energy difference of the association process as a function of $-\Delta$SESA. (b) The corresponding change in the entropy, $T\Delta S$, of the system.

associated state,

$$\Delta G_{\text{direct}} = \sum_{i=1}^{N} u_i \qquad (4)$$

The sum in eq 4 is over all particles on one of the sheets, and u_i is the interaction energy of particle i on that sheet with all particles on the other sheet. If u_i is constant for all i then ΔG_{direct} will scale with the surface area. However, particles at the edge will have weaker interactions than particles in the middle of the plates, and the fraction of the former decreases with the size of the hydrophobes. This explains why $\Delta G_{\text{total}}/(-\Delta\text{SESA})$ in Figure 3a continues to go down (toward stronger interactions) with an increase in N. Nevertheless, above a certain size of the sheets the fraction of the edge particles will not contribute significantly to the sum in eq 4 and ΔG_{total} will scale with the change in the surface area. The values of the curves at large N indicate that upon association of graphene sheets there is a water-induced stabilization of ~12 kJ/mol per 1 nm^2 area of the sheets, and the total stabilization can be extrapolated to approximately 65 kJ/mol/nm^2.

dx.doi.org/10.1021/jp1090284 |J. Phys. Chem. B 2011, 115, 2303–2311

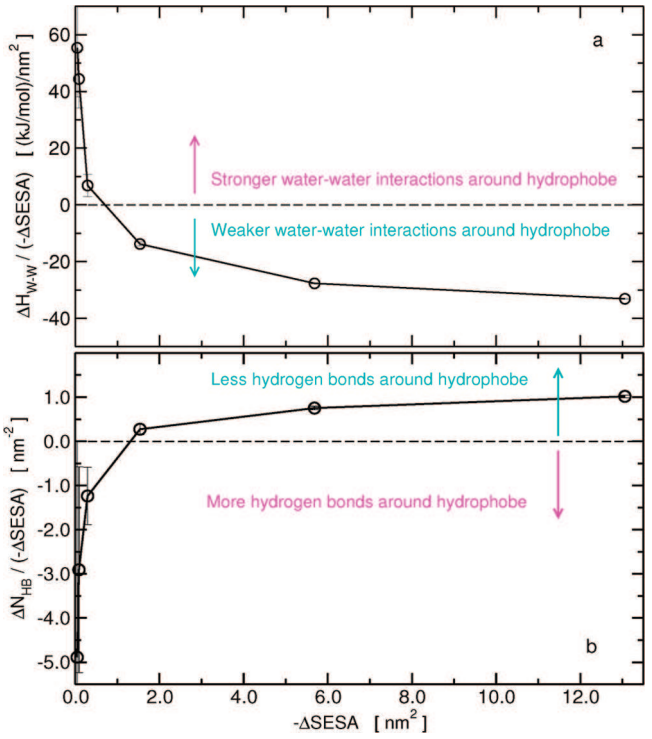

Figure 4. (a) Change in enthalpy between the solvent water molecules, ΔH_{W-W}, for the association process, and (b) the change in the number of hydrogen bonds as a function of the change in the surface area exposed to the solvent.

The change in the entropy of the system scaled by $-\Delta$SESA is plotted in Figure 3b. This entropy change represents the change in the entropy of the (interfacial) water molecules since the hydrophobes degrees of freedom are frozen. The scaled entropy change also reaches a constant value, however, the plateau region starts only at $N = 104$. The curve indicates that relative to the surface area that is buried in the reaction, $T\Delta S$ is larger for smaller hydrophobes (which also can be inferred from Table 3). For the same reason ΔG_{direct} does not scale with the change in the surface area, ΔH does not scale as well (graph not shown). We, therefore, plotted the change in enthalpy between the water molecules for the association process, ΔH_{W-W}, in Figure 4a (the change in the water−solute enthalpy scaled by $-\Delta$SESA is shown in Figure 2 of the Supporting Information). Similar to the behavior of ΔH of the system, ΔH_{W-W} is positive for $N \leq 6$, which means that the reorganization energy between water molecules around the hydrophobes opposes hydrophobic association. This is possible if the hydrogen-bonding energy between water molecules surrounding small hydrophobic solutes is larger than that in bulk water. There are conflicting reports in the literature in regard to the behavior of hydrogen bonds around small solutes. In one study, it is argued that within the first shell around small hydrophobes the distortions of hydrogen bonds from ideal geometry are smaller than in bulk,[35] while in another study it is claimed that small hydrophobic groups are surrounded by a loose, hydrogen-bonded cage of water molecules.[36] In Figure 4b, the change in the number of hydrogen bonds in the entire system is plotted as a function of $-\Delta$SESA. The graph shows that for $N \leq 6$ more hydrogen bonds between the water molecules are found in the dissociated state than in the associated state, and vice versa for $N \geq 28$. Thus, around small hydrophobic solutes there are more, while around large hydrophobes there are less, hydrogen bonds than in bulk. The value of the curve at large N indicates that on average there is an increase of about one hydrogen bond per 1 nm^2 of graphene sheet association.

Bulk water molecules do not attain the maximum energy of interaction with their neighbors due to thermal excitations and the constant rearrangement of their hydrogen bond network. As a result, the average number of hydrogen bonds per water molecules at room temperature is smaller than four.[37−40] However, these structural defects facilitate water reorientations and hydrogen bonds rearrangements[41−44] and thereby augment the entropy. The reorientation time of water molecules around hydrophobic solutes is known to be retarded relative to the bulk.[41,45−51] Is there, then, a difference in the slowing down of the water dynamics around small hydrophobes compared to large hydrophobes? In Figure 5a we plotted the autocorrelation function of the hydrogen bonds, $C_{HB}(t)$, allowing bond breaking at intermediate times, while in the calculation of the correlation in Figure 5b, $S_{HB}(t)$, the hydrogen bonds are present continuously (see Methods section). This was performed for $N = 1$ and 240, at gap separation of $d = 1.86$ nm (i.e., the dissociated state where the plates do not influence each other), as well as for bulk water. The results show that around small solutes the relaxation of both correlation functions is slower than in the bulk, indicating that the hydrogen bonds are more long-lived and rearrange slower. The fact that these hydrogen bonds break less frequently than in bulk is the reason why there is an enthalpic gain, and an increase in the number of hydrogen bonds, for solvating small hydrophobes in water (the positive enthalpies in Table 3 and the negative values of ΔN_{HB} in Figure 4b). Even when they break, there is a higher probability to re-form a hydrogen bond between the same pair of water molecules. This can be attributed to the tangential orientation of the hydrogen bonds in the first solvation shell around small solutes[35,36] that restrict the possibilities of rearranging their network. Around large hydrophobes, on the other hand, only the relaxation of $C_{HB}(t)$ is retarded compared to bulk water. This means that, although the hydrogen bond lifetime is not longer, the rearrangement of the hydrogen bonds network is slower than in bulk (since the hydrogen bonds are reformed with the same neighbors). We conjecture that the difference in the behavior between small and large solutes stems from the fact that at the interface with large hydrophobes there is a decrease in the number of hydrogen bonds (see Figure 4b) rendering the breaking of individual bonds easier ($S_{HB}(t)$ relaxes faster). However, the oscillations in density[34,52,53] and the strong preferential orientation[34,52,54−57] exhibited by water molecules at these surfaces reduce the possibilities of rearranging the hydrogen bonds network; thus, the relaxation of $C_{HB}(t)$ is similar to that around small hydrophobes and slower than in bulk.

The diffusion of water molecules next to hydrophobes is also known to be retarded.[58−60] In Figure 5c we display the mean squared displacement of the water molecules in the xy-plane (parallel to the graphene surface) around $N = 1$ and $N = 240$ as well as in bulk. The plots cover short times (the two-dimensional diffusion coefficients, D, were calculated in the range of 2−18 ps) since for longer times the water will diffuse away from the hydrophobe. The figure indicates that water molecules in the bulk diffuse faster than around hydrophobic solutes. As is the case for the relaxation of the hydrogen bond correlation function, $C_{HB}(t)$, the plots for $N = 1$ and $N = 240$ are very similar. Thus, the reorientation time and diffusion are slower for water molecules surrounding a carbon atom than they are in bulk. This can be

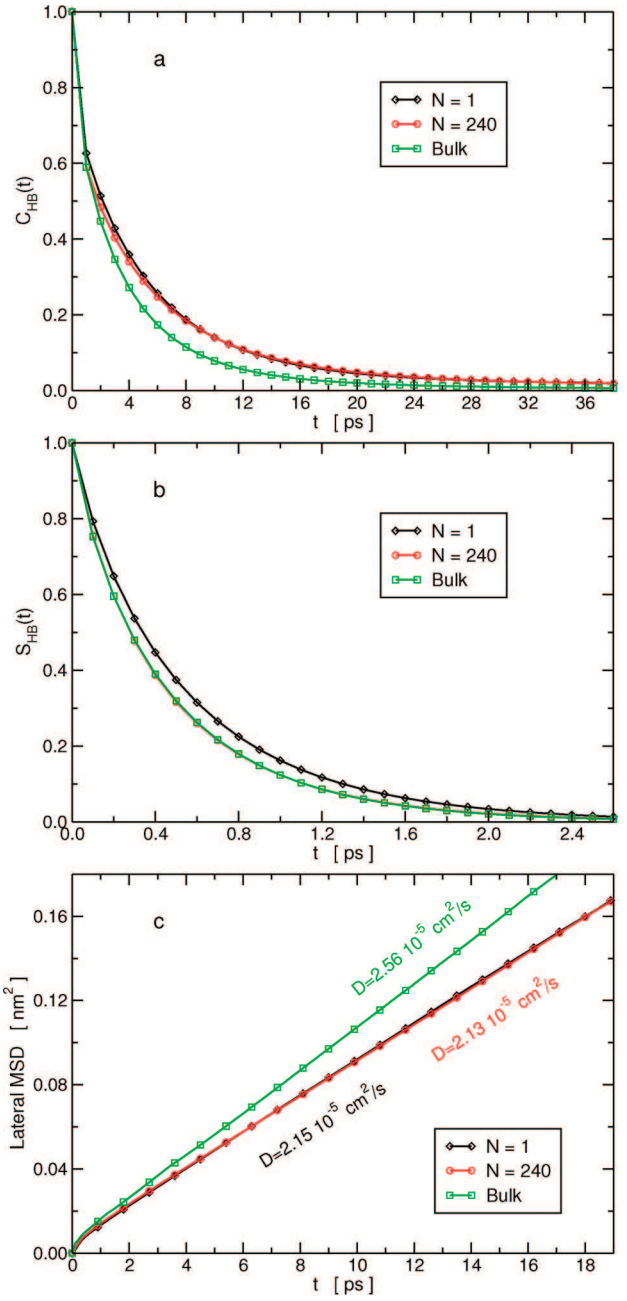

Figure 5. Hydrogen bond lifetime between water molecules next to the hydrophobe and in bulk. In (a) the autocorrelation function, $C_{HB}(t)$, counts also re-formed bonds (as defined in eq 1), while in (b) the autocorrelation $S_{HB}(t)$ counts bonds that are only continuously existing (defined in eq 2). In the latter, the curves for $N = 240$ and the bulk are very similar. (c) The mean-squared displacement of the water molecules in the *xy*-plane around the hydrophobe and in bulk, and the corresponding two-dimensional diffusion constants. In all cases, the analysis was performed around each plate in the dissociated state ($d = 1.86$ nm).

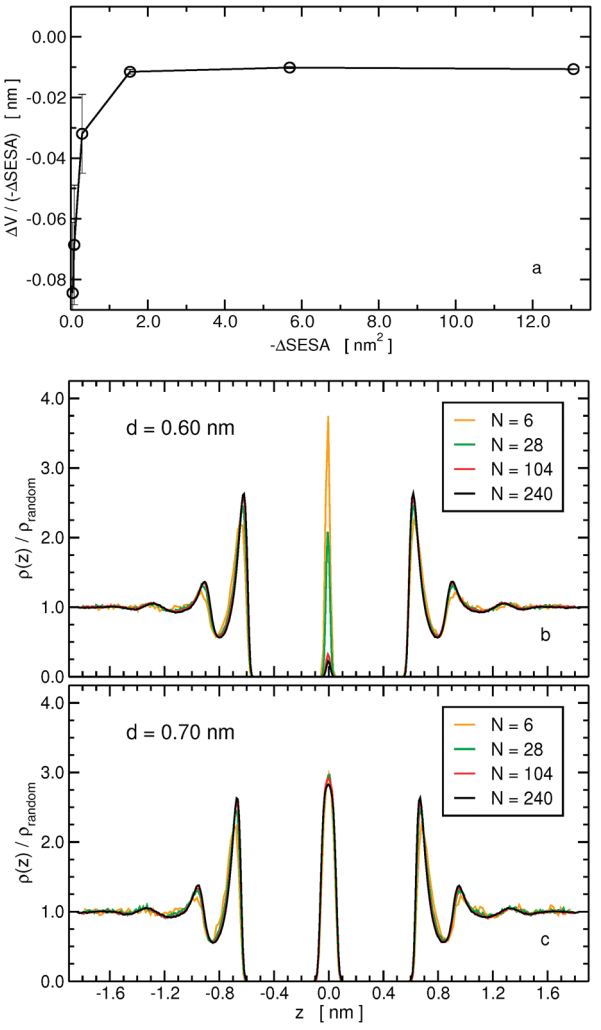

Figure 6. (a) Change in the total volume of the system for the association process as a function of −ΔSESA. (b) Density profile of the (oxygen atoms of) water molecules along the *z*-axis (which is perpendicular to the plane of the graphene sheets), divided by the average water density, at $d = 0.60$ nm. (c) Same as (b) but for $d = 0.70$ nm.

explained through the mechanism of breaking a hydrogen bond between water molecules. In order to diffuse or rotate, a water molecule has to break some of the hydrogen bonds that it makes with its neighbors. Since the strength of a hydrogen bond is much larger than the magnitude of thermal fluctuations, it is unlikely that a hydrogen bond will be broken without lowering its barrier height. Such a mechanism has been reported in the literature[41−43] in which a water molecule can break a hydrogen bond by accepting a fifth water molecule to its first solvation shell forming a bifurcated hydrogen bond. A water molecule surrounding a carbon atom still has approximately four water molecules in its first solvation shell. Therefore, it has lower possibilities that a fifth water molecule from the second solvation shell will be able to enter its first shell. As a consequence, the rate of breaking hydrogen bonds, and thereby the rotation and diffusion, of this molecule are slower than in bulk.[61]

The existence of a thin vapor layer, or density fluctuations, around extended hydrophobic surfaces has been proposed[7] and reported experimentally for a hydrocarbon system.[62] However, other studies found no evidence for such behavior in systems that are characterized even by a weak water−surface attractive interactions.[63−65] Analysis of the density profiles of the water molecules along the axis perpendicular to the water/hydrophobe interface in our model systems indicates stratification with a pronounced first peak (see for example, the density profile for $|z| > 0.5$ nm in Figure 6, b and c) precluding the possibility of a vapor

dx.doi.org/10.1021/jp1090284 |*J. Phys. Chem. B* 2011, 115, 2303–2311

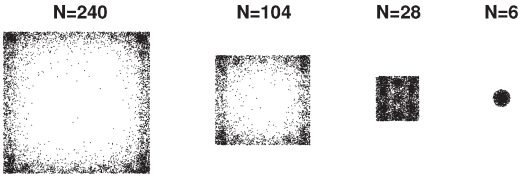

Figure 7. Superposition of the water coordinates projected on the *xy* plane for $d = 0.60$ nm. For clarity, only water molecules that are present between the plates are shown (see Table 1 for the dimensions of the rectangular cuts, whereas for $N = 6$, a circular cutoff with a radius of 0.142 nm was taken). In all cases, the superposition is composed of 4200 frames with a time interval of 10 ps.

layer. Nevertheless, the change in the total volume of the system, ΔV, for association is negative. This is a result of the fact that the hydrophobe−water contact distance is larger than the water−water and hydrophobe−hydrophobe contact distances. The value of ΔV scaled by the surface area that is eliminated is shown in Figure 6a. A clear scalability with the change in the surface area of the hydrophobe is observed, implying that extrapolation to larger surfaces would yield interfacial waters with structure that is similar to that obtained in this study.

A different situation occurs for water molecules that are confined between the two plates. The first maximum in the PMFs shown in Figure 2 is the Gibbs energy barrier for removing the last layer of water between the two surfaces. For $N = 104$, it is located at a gap separation of 0.60 nm. The density of waters along the *z*-axis for $N = 6$, 18, 104, and 240 at $d = 0.60$, and 0.70 nm is plotted in Figure 6, panels b and c, respectively. The graph indicates that for $d = 0.60$ nm the water density between the two surfaces ($|z| < 0.2$ nm) is reduced with increasing the plate size. We therefore plotted in Figure 7 a superposition of the coordinates of these interplate water molecules projected on the *xy* plane. The water molecules in the $N = 6$, 28 systems exhibit a different behavior than in the $N = 104$, 240 systems. While for the smaller plates the water molecules reside throughout the interplate lateral projected region (although inhomogeneity is already noticeable at $N = 28$), for the larger plates the water molecules exhibit much higher probability at the edges, and especially the corners, of the plates. Note that, in all cases, an instantaneous configuration of the interplate region can be an empty state that gradually increases in the number of the confined water molecules (see Figure 1 in the Supporting Information). The decrease in stability of the confined liquid water for larger *N* is the reason why the scaled (induced) PMFs in the range $d < 0.64$ nm display a relatively lower barrier for association and larger range of attraction as *N* increases (see Figure 2, lower panel). On the other hand, for $d = 0.70$ nm, where the scaled PMFs for $N = 28$, 104, and 240 exhibit approximately the same value, the density of the water molecules between the two plates is very similar (Figure 6c) and homogeneous in the projection on the *xy* plane (plots not shown).

IV. CONCLUSIONS

In this paper we performed computer simulations aiming to obtain the thermodynamics of the hydrophobic interaction at different length scales. The model systems chosen represent rectangular cuts of a graphene sheet. It is shown that for small solutes the attractive interaction is purely entropic. In fact, enthalpy favors the dissociated state because there are more hydrogen bonds around small solutes than in bulk. Above a critical value of the change in surface area of the hydrophobe in the association process (which we found to be in the range of 0.3−1.5 nm^2), enthalpy enters as a second driving force for attraction. With further increase of this change in surface area, the relative contribution of enthalpy increases and become the dominant factor. For the largest graphene sheets we studied, 70% of the change in Gibbs energy for association is enthalpic. Increasing the plate size further is likely to exhibit a convergence in the distribution of the Gibbs energy components (probably not too far from the 7:3 ratio). These results are in sharp contrast with previous molecular dynamics simulations which found the driving force for nanoscopic graphene sheets association to be purely entropic.[66] Note that, in these simulations, the PMF as well as the enthalpy and entropy were calculated by different methods than those employed here.

The difference between small- and large-scale association is the inability of the water molecules at the interface with large surface to maintain their hydrogen bond network. We find that on average one hydrogen bond is broken around 1 nm^2 hydrophobic surface. The water-induced Gibbs energy for graphene sheet association is about −12 kJ/mol/nm^2, and is not the major factor in the total stabilization (which is about −65 kJ/mol/nm^2). From this point of view, graphene sheets are not fully representative for "hydrocarbon-like" system. Nevertheless, the water-induced Gibbs energy for graphene sheets association is negative as opposed to positive values obtained recently for bicyclooctane, adamantane, and fullerene systems.[67] It is very likely that the strong LJ dispersion interactions between these hydrophobes and water[68] as well as the convex shape of their hydrophobic surface[69] are responsible for the fact that in these systems water opposes association.

Furthermore, we showed that hydrogen bonds around small hydrophobes live longer than in the bulk, explaining their larger number around these solutes. Hydrogen-bond rearrangement is also retarded in this case. On the other hand, around large hydrophobes, the hydrogen bond lifetime is similar to that in the bulk; however, the dynamics of rearranging the network is slower. In the large-scale regime, the PMF of graphene sheets can be scaled to yield a master curve, except for $d < 0.64$ nm, thus, around the barrier of removing the last water layer. The decrease in stability of the water molecules (in the liquid state) in this confined gap with increasing plate size rationalizes the different behavior of the scaled PMFs in this region. As a consequence, a relatively lower barrier height for association and larger range of attraction is observed for larger surfaces.

■ ASSOCIATED CONTENT

Ⓢ Supporting Information. Figures of the instantaneous number of water molecules between the two graphene sheets and the change in enthalpy between water molecules and the hydrophobic solutes. This material is available free of charge via the Internet at http://pubs.acs.org.

■ AUTHOR INFORMATION

Corresponding Author
*E-mail: r.zangi@ikerbasque.org.

■ ACKNOWLEDGMENT

This work has been funded with support from the European Commission, Marie Curie International Reintegration Grant,

project no. 247485. Technical and human support provided by SGIker (USED SERVICES) (UPV/EHU, MICINN, GV/EJ, ESF) is gratefully acknowledged. The author also thankfully acknowledges the computer resources and technical assistance provided by the Barcelona Supercomputing Center—Centro Nacional de Supercomputación.

REFERENCES

(1) Kauzmann, W. *Adv. Protein Chem.* **1959**, *14*, 1–63.
(2) Miller, K. W.; Hildebrand, J. H. *J. Am. Chem. Soc.* **1968**, *90*, 3001–3004.
(3) Butler, J. A. V. *Trans. Faraday Soc.* **1937**, *33*, 229–238.
(4) Blokzijl, W.; Engberts, J. B. F. N. *Angew. Chem., Int. Ed. Engl.* **1993**, *32*, 1545–1579.
(5) Frank, H. S.; Evans, M. W. *J. Chem. Phys.* **1945**, *13*, 507–532.
(6) Stillinger, F. H. *J. Solution Chem.* **1973**, *2*, 141–158.
(7) Lum, K.; Chandler, D.; Weeks, J. D. *J. Phys. Chem. B* **1999**, *103*, 4570–4577.
(8) Huang, D. M.; Geissler, P. L.; Chandler, D. *J. Phys. Chem. B* **2001**, *105*, 6704–6709.
(9) Rajamani, S.; Truskett, T. M.; Garde, S. *Proc. Natl. Acad. Sci. U.S. A.* **2005**, *102*, 9475–9480.
(10) Graziano, G. *J. Phys. Chem. B* **2006**, *110*, 11421–11426.
(11) Glew, D. N. *J. Phys. Chem.* **1962**, *66*, 605–609.
(12) Head-Gordon, T. *Proc. Natl. Acad. Sci. U.S.A.* **1995**, *92*, 8308–8312.
(13) Bowron, D. T.; Filipponi, A.; Roberts, M. A.; Finney, J. L. *Phys. Rev. Lett.* **1998**, *81*, 4164–4167.
(14) Chandler, D. *Nature* **2002**, *417*, 491.
(15) Chandler, D. *Nature* **2005**, *437*, 640–647.
(16) Werder, T.; Walther, J.; Jaffe, R.; Halicioglu, T.; Koumoutsakos, P. *J. Phys. Chem. B* **2003**, *107*, 1345–1352.
(17) Hess, B.; Kutzner, C.; van der Spoel, D.; Lindahl, E. *J. Chem. Theory Comput.* **2008**, *4*, 435–447.
(18) Horn, H. W.; Swope, W. C.; Pitera, J. W.; Madura, J. D.; Dick, T. J.; Hura, G. L.; Head-Gordon, T. *J. Chem. Phys.* **2004**, *120*, 9665–9678.
(19) Miyamoto, S.; Kollman, P. A. *J. Comput. Chem.* **1992**, *13*, 952–962.
(20) Bussi, G.; Donadio, D.; Parrinello, M. *J. Chem. Phys.* **2007**, *126*, 014101.
(21) Berendsen, H. J. C.; Postma, J. P. M.; van Gunsteren, W. F.; DiNola, A.; Haak, J. R. *J. Chem. Phys.* **1984**, *81*, 3684–3690.
(22) Pangali, C. S.; Rao, M.; Berne, B. J. In *Computer Modeling of Matter*; Lykos, P., Ed.; ACS Symposium Series No. 86; American Chemical Society: Washington, DC, 1978; p 29.
(23) Zangi, R.; Zhou, R.; Berne, B. J. *J. Am. Chem. Soc.* **2009**, *131*, 1535–1541.
(24) Flyvbjerg, H.; Petersen, H. G. *J. Chem. Phys.* **1989**, *91*, 461–466.
(25) Sanner, M. F.; Olson, A. J.; Spehner, J.-C. *Biopolymers* **1996**, *38*, 305–320.
(26) Luzar, A.; Chandler, D. *Phys. Rev. Lett.* **1996**, *76*, 928–931.
(27) Pal, S.; Maiti, P. K.; Bagchi, B. *J. Chem. Phys.* **2006**, *125*, 234903.
(28) Bérard, D. R.; Attard, P.; Patey, G. N. *J. Chem. Phys.* **1993**, *98*, 7236–7244.
(29) Wallqvist, A.; Berne, B. J. *J. Phys. Chem.* **1995**, *99*, 2893–2899.
(30) Leung, K.; Luzar, A.; Bratko, D. *Phys. Rev. Lett.* **2003**, *90*, 065502.
(31) Zangi, R.; Hagen, M.; Berne, B. J. *J. Am. Chem. Soc.* **2007**, *129*, 4678–4686.
(32) Hua, L.; Zangi, R.; Berne, B. J. *J. Phys. Chem. C* **2009**, *113*, 5244–5253.
(33) Huang, X.; Zhou, R.; Berne, B. J. *J. Phys. Chem. B* **2005**, *109*, 3546–3552.
(34) Choudhury, N.; Pettitt, B. M. *J. Am. Chem. Soc.* **2005**, *127*, 3556–3567.
(35) Raschke, T. M.; Levitt, M. *Proc. Natl. Acad. Sci. U.S.A.* **2005**, *102*, 6777–6782.
(36) Soper, A. K.; Luzar, A. *J. Phys. Chem.* **1996**, *100*, 1357–1367.
(37) Chandra, A. *Phys. Rev. Lett.* **2000**, *85*, 768–771.
(38) Myneni, S.; Luo, Y.; Näslund, L. Å.; Cavalleri, M.; Ojamäe, L.; Ogasawara, H.; Pelmenschikov, A.; Wernet, P.; Väterlein, P.; Heske, C.; Hussain, Z.; Pettersson, L. G. M.; Nilsson, A. *J. Phys.: Condens. Matter* **2002**, *14*, L213–L219.
(39) Smith, J. D.; Cappa, C. D.; Wilson, K. R.; Messer, B. M.; Cohen, R. C.; Saykally, R. J. *Science* **2004**, *306*, 851–853.
(40) Zangi, R. *J. Phys. Chem. B* **2010**, *114*, 643–650.
(41) Sciortino, F.; Geiger, A.; Stanley, H. E. *Nature* **1991**, *354*, 218–221.
(42) Laage, D.; Hynes, J. T. *Science* **2006**, *311*, 832–835.
(43) Laage, D.; Hynes, J. T. *J. Phys. Chem. B* **2008**, *112*, 14230–14242.
(44) Tay, K. A.; Bresme, F. *Phys. Chem. Chem. Phys.* **2009**, *11*, 409–415.
(45) Geiger, A.; Rahman, A.; Stillinger, F. H. *J. Chem. Phys.* **1979**, *70*, 263–276.
(46) Rossky, P. J.; Karplus, M. *J. Am. Chem. Soc.* **1979**, *101*, 1913–1937.
(47) Carlstroem, G.; Halle, B. *Langmuir* **1988**, *4*, 1346–1352.
(48) Ishihara, Y.; Okouchi, S.; Uedaira, H. *J. Chem. Soc., Faraday Trans.* **1997**, *93*, 3337–3342.
(49) Xu, H.; Berne, B. J. *J. Phys. Chem. B* **2001**, *105*, 11929–11932.
(50) Rezus, Y. L. A.; Bakker, H. J. *Phys. Rev. Lett.* **2007**, *99*, 148301.
(51) Laage, D.; Stirnemann, G.; Hynes, J. T. *J. Phys. Chem. B* **2009**, *113*, 2428–2435.
(52) Lee, C. Y.; McCammon, J. A.; Rossky, P. J. *J. Chem. Phys.* **1984**, *80*, 4448–4455.
(53) Zangi, R. *J. Phys.: Condens. Matter* **2004**, *16*, S5371–S5388.
(54) Scatena, L. F.; Brown, M. G.; Richmond, G. L. *J. Phys. Chem. B* **2001**, *105*, 11240–11250.
(55) Zangi, R.; Engberts, J. B. F. N. *J. Am. Chem. Soc.* **2005**, *127*, 2272–2276.
(56) Hore, D. K.; Walker, D. S.; MacKinnon, L.; Richmond, G. L. *J. Phys. Chem. C* **2007**, *111*, 8832–8842.
(57) Zangi, R.; Berne, B. J. *J. Phys. Chem. B* **2008**, *112*, 8634–8644.
(58) Lee, S. H.; Rossky, P. J. *J. Chem. Phys.* **1994**, *100*, 3334–3345.
(59) Haselmeier, R.; Holz, M.; Marbach, W.; Weingaertner, H. *J. Phys. Chem.* **1995**, *99*, 2243–2246.
(60) Hua, L.; Huang, X.; Zhou, R.; Berne, B. J. *J. Phys. Chem. B* **2006**, *110*, 3704–3711.
(61) Bakulin, A. A.; Liang, C.; la Cour Jansen, T.; Wiersma, D. A.; Bakker, H. J.; Pshenichnikov, M. S. *Acc. Chem. Res.* **2009**, *42*, 1229–1238.
(62) Jensen, T. R.; Jensen, M. Ø.; Reitzel, N.; Balashev, K.; Peters, G. H.; Kjaer, K.; Bjørnholm, T. *Phys. Rev. Lett.* **2003**, *90*, 086101.
(63) Takata, Y.; Cho, J.-H. J.; Law, B. M.; Aratono, M. *J. Am. Chem. Soc.* **2006**, *22*, 1715–1721.
(64) Choudhury, N.; Pettitt, B. M. *J. Am. Chem. Soc.* **2007**, *129*, 4847–4852.
(65) Choudhury, N. *J. Chem. Phys.* **2009**, *131*, 014507.
(66) Choudhury, N.; Pettitt, B. M. *J. Phys. Chem. B* **2006**, *110*, 8459–8463.
(67) Makowski, M.; Czaplewski, C.; Liwo, A.; Scheraga, H. A. *J. Phys. Chem. B* **2010**, *114*, 993–1003.
(68) Graziano, G. *Chem. Phys. Lett.* **2010**, *499*, 79–82.
(69) Wallqvist, A.; Berne, B. J. *J. Phys. Chem.* **1995**, *99*, 2885–2892.

Supporting Information:

Driving Force for Hydrophobic Interaction at Different Length-Scales

Ronen Zangi[1,2]

1. Department of Organic Chemistry I, University of the Basque Country UPV/EHU, Avenida de Tolosa 72, 20018, San Sebastian, Spain

2. IKERBASQUE, Basque Foundation for Science, 48011, Bilbao, Spain

Email: r.zangi@ikerbasque.org

January 20, 2011

Figures

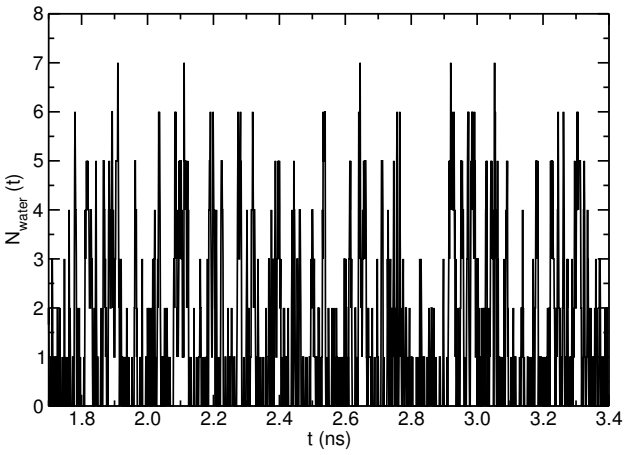

Figure 1: The instantaneous number of water molecules between the two graphene sheets for N=28 as a function of time. The graph, which displays a short segment of the trajectory, indicates that an instantaneous configuration of the interplate region can be an empty state that gradually increases in the number of the confined water molecules.

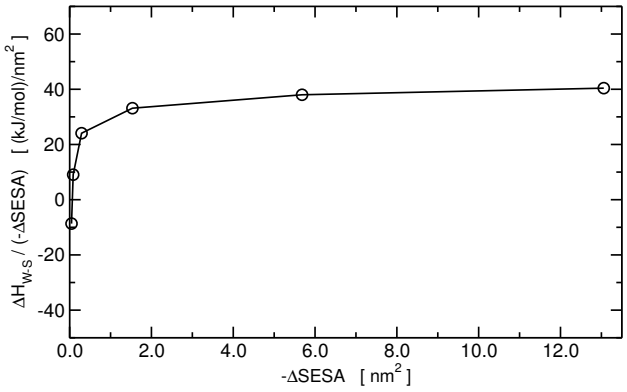

Figure 2: The change in enthalpy between water molecules and the hydrophobic solutes, $\Delta H_{\mathrm{W-S}}$, for the association process, scaled by the change in the surface area of the hydrophobes exposed to the solvent (-ΔSESA).